Applied Nanoscience
https://doi.org/10.1007/s13204-021-01998-y

ORIGINAL ARTICLE

Design of various Ni–Cr nanostructures and deducing their magnetic anisotropy

Murtaza Bohra[1,2] · Sai Vittal Battula[1] · Vidya Alman[1] · Anil Annadi[1] · Vidyadhar Singh[2,3,4]

Received: 12 May 2021 / Accepted: 19 July 2021

Abstract

Understanding the effects of interparticle interactions is a vital problem because magnetic nanoparticles showcase a variety of magnetic configurations due to different contributions to their total energy. To derive reliable and robust properties from magnetic nanoparticles, it is, thus, necessary to understand the competition between particle anisotropy and interparticle interactions that define the magnetic state of nanoparticles, where size control plays an important role. Here, we apply the random anisotropy model (RAM) that considers various magnetic interactions to selectively prepared NiCr nanostructures (NiCr dense nanoclusters, nanogranular NiCr thin films, and Ag(NiCr) nanocomposites) with different interparticle interactions. The estimated single-particle magnetic anisotropy K values ($2.82-12.3\times10^4$ J/m^3) and careful analysis of magnetization behavior for these nanostructures reveal that orbital hybridization, surface segregation, and interface character govern the magnetic interactions among nanoparticles. Our study demonstrates how magnetic behaviors vary in these different magnetic systems consisting of superparamagnetic (SPM) and ferromagnetic (FM) contributions specific to magnetic interactions. AQ1

Keywords Magnetic anisotropy · NiCr nanoalloy · Random anisotropy model (RAM) · Blocking temperature

Introduction

Mutual interactions among magnetic nanoparticles demonstrate immense importance in the understanding of collective magnetic behaviors (Fabris et al. 2019; Ridier et al. 2017a; Mørup et al. 2010; Bitoh et al. 2003; Petracic et al. 2006; Pacakova et al. 2016). Experimentally, it is observed that magnetic interactions depend on various factors such as particle size, shape, interparticle separation, and also the chemical composition that control spin structure at the nanoscale, (Andersson et al. 2015; Muscas et al. 2018). Theoretical description of the magnetic behavior of single-domain systems is usually described by a superparamagnetic (SPM) framework which often undermines interaction effects (Nunes et al. 2005). Though few existing models consider magnetic interaction effects, there is a scarcity in determining the magnetic stability of single-domain magnetic nanoparticles against temperature and switching field distribution (Fabris et al. 2019). In single-domain magnetic nanoparticles, magnetic anisotropy competes with interparticle interactions in determining the orientation of the particle moments (Nunes et al. 2005). The type of interparticle interactions depends on particle properties (particle concentration and size distribution) and the medium surrounding these particles (Nunes et al. 2005; Denardin et al. 2006; Knobel et al. 2007; Knobel et al. 2008). For instance, when the system is dominated by dipole–dipole interactions, a disordered collective state or spin cluster glass is expected, whereas a ferromagnetic state can be formed when the interactions are dominated by exchange coupling as the particles are in direct contact or dispersed in a ferromagnetic amorphous matrix. These facts open the possibility to analyze the effect of interaction-induced variations on superparamagnetic properties. Recently, researchers proposed a modified random anisotropy model (RAM) (Nunes et al. 2005; Denardin et al.

✉ Murtaza Bohra
murtazaphy@gmail.com

[1] Mahindra University École Centrale School of Engineering (MEC), Survey Number 62/1A, Bahadurpally Jeedimetla, Hyderabad 500043, Telangana, India

[2] Okinawa Institute of Science and Technology Graduate University, Tancha Onna-Son, 1919-1 Tancha Onna-Son, Okinawa 904-0495, Japan

[3] University Department of Physics, Jai Prakash University, Chapra 841301, Bihar, India

[4] Department of Physics, Ram Jaipal College, Jai Prakash University, Chapra 841301, Bihar, India

2006; Knobel et al. 2007; Andersson et al. 2015), which considers the collective behavior of nanoparticles such as the concentration and particle size, as well as the magnetic correlation length. To verify the universality of this model regardless of the nature of the interactions, such as direct exchange, dipole–dipole, and indirect exchange Ruderman–Kittel–Kasuya–Yosida (RKKY) (Denardin et al. 2006; Knobel et al. 2007; Knobel et al. 2008; Bohra et al. 2015), it has to be examined in more complex ensembles of magnetic nanostructures, with the same size but with different interaction strength. In this study, NiCr nanostructures (in the form of nanoclusters, nanogranular films, and nanocomposites), which offer a plethora of diverse applications (magnetic hyperthermia, magnetic resonance imaging, and magnetic data storage) (Bohra et al. 2016; 2017), as compared to the oxide nanoparticles (Dhayal et al. 2020; Kumar et al. 2021; Kumari et al. 2021), are selected as a model system for the investigation of competition between single-particle magnetic anisotropy and and interparticle interactions.

Experiment

Three different types of NiCr nanostructures were grown on Si substrates at room temperature. Detail growth conditions for these samples are as follows:

1. Pure Ni and $Ni_{0.95}Cr_{0.05}$ nanoclusters (NCs): The controlled size growth of theseNCs were achieved by cluster beam deposition using magnetron sputtering inert-gas condensation (Nanogen50 Source, Mantis Deposition Ltd., UK) unit at a DC sputtering power of 40 W from Ni and $Ni_{0{\cdot}95}Cr_{0.05}$ alloy targets (purity 99.999%) procured from Kurt J. Lesker Company (Bohra et al. 2015; Bohra et al. 2016; Bohra et al. 2017) Constant pressures were maintained at 2.5×10^{-1} mbar in the aggregation zone and 6×10^{-4} mbar in the main chamber with constant argon (Ar) flow rate set at 60 sccm and helium (He) flow rate at 5 sccm. These NCs (~5 nm sizes) show the nominal composition of bulk target alloy ($Ni_{0.95}Cr_{0.05}$) with slight Cr surface segregations, shown in Supplementary information Figs. S1–S3. Further, as grown $Ni_{0.95}Cr_{0.05}$ NCs were annealed in a high vacuum of 10^{-8} mbar at 450 °C. These annealed NCs show pronounced Cr segregations with slight particle size growth (Figs. S4–S 6) (Bohra et al. 2020).
2. Ag(NiCr) nanocomposites: The nanocomposites were grown by co-sputtering of Ag and $Ni_{0.95}Cr_{0.05}$ targets at DC powers of 20 and 40 W, respectively, in argon pressure of 6.0×10^{-4} mbar (Bohra et al. 2016). Nanocomposites show the atomic composition of Ag (65%) and $Ni_{0.95}Cr_{0.05}$ (35%) with an average $Ni_{0.95}Cr_{0.05}$ size of ~5 nm (Figs. S7–S8). The micro-strain produced in the $Ni_{0.95}Cr_{0.05}$ nanostructures embedded in the Ag matrix is about 0.036, estimated from the XRD data (Kaushik et al. 2013; Punia et al. 2021a, 2021b), is slightly higher than $Ni_{0.95}Cr_{0.05}$ NCs (0.026) and $Ni_{0.95}Cr_{0.05}$ nanogranular thin films (0.022).
3. $Ni_{0.95}Cr_{0.05}$nanogranular thin films: These were deposited by conventional sputtering of $Ni_{0{\cdot}95}Cr_{0.05}$ alloy target at the DC power of 40 W. These films show nanocrystalline nature with an average grain size of ~5 nm (Fig. S9).

The grazing incidence X-ray diffraction (GIXRD) data were collected using a Bruker D8 Discover XRD2 system with a Cu Ka X-ray source (operated at 40 kV and 40 mA) to check crystalline phases. The surface morphology and coverage of these samples were characterized by atomic force microscopy (AFM). Ultrathin carbon film and silicon nitride (Si_3N_4) membrane TEM grids were used as substrates for TEM and STEM analysis, using a Cs-corrected environmental TEM (FEI Titan G2 80–300 kV) operating at 300 kV. Energy dispersive X-ray (EDX) analysis was done to confirm the composition of the samples, and electron energy loss spectroscopy (EELS) elemental mapping was performed to elucidate the structural changes of the nanoalloys. Magnetic properties were measured using a vibrating sample magnetometer (VSM) attached to the physical property measurement system (PPMS), and magnetic moments were extracted after correcting for the diamagnetic contribution of the Si substrate. M–H loops were measured over the range of 5–400 K. For zero-field-cooled (ZFC) magnetization, the sample was initially cooled to 5 K in zero fields and then magnetization was measured in the presence of a fixed field upon heating. Subsequently, in the same field, the field-cooled (FC) magnetization was recorded during cooling.

Results and discussion

Figure 1(a) shows the TEM image for one of the representative samples of $Ni_{0.95}Cr_{0.05}$ nanoclusters which confirm the nanocluster formation with a particle average size of 5 nm. Note that the low coverage sample of $Ni_{0.95}Cr_{0.05}$ is used for TEM purposes; however, high-density samples were used for the magnetic study that has ~35% volume coverage of $Ni_{0.95}Cr_{0.05,}$ as estimated by EDAX and sputtering growth rate analysis (Fig. S3, S5, S8 and S9). The selected area diffraction pattern (Fig. 1(b)) of this sample confirms the formation of single-phase face-centered-cubic (fcc) $Ni_{0.95}Cr_{0.05}$ with lattice constant 3.5 Å.

Interparticle interaction effects can be identified by analysis of the blocking temperature (T_B) obtained from magnetization behavior such as the zero-field-cooled (ZFC) and field-cooled (FC) curves as a function of temperature, as shown

Journal : Large 13204 | Article No : 1998 | Pages : 7 | MS Code : 1998 | Dispatch : 7-8-2021

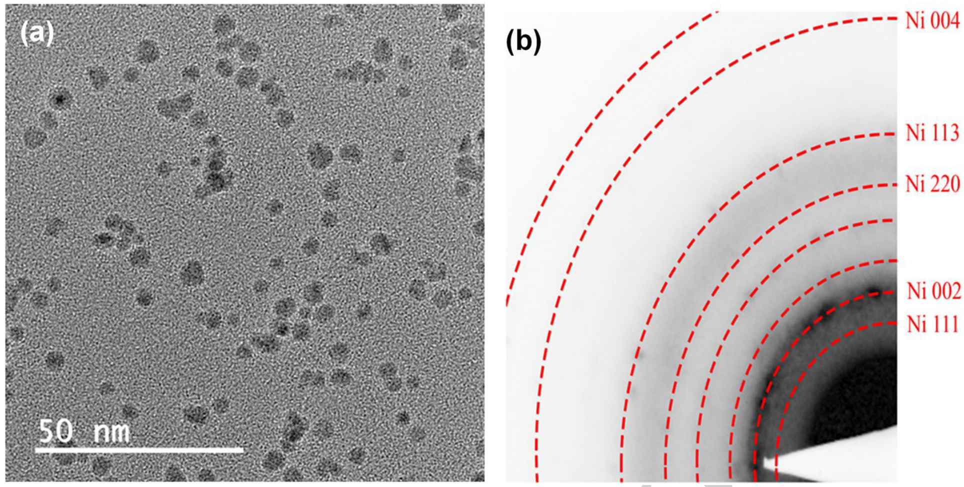

Fig. 1 **a** TEM image of $Ni_{0.95}Cr_{0.05}$ nanoclusters and its **b** Selected area diffraction pattern

in Fig. 2(a–e) at different fields H (50 − 1 kOe) for various types of NiCr nanostructures. The maximum of the ZFC curves (indicated by the red arrow) related to the mean T_B, shift toward lower temperatures on increasing H. The different value of T_B at a fixed field in different samples is indeed a strong signature for a different level of interparticle magnetic interactions among NiCr nanostructures. In non-interacting single-domain magnetic systems, the effect of H on the T_B is generally expressed by (Nunes et al. 2005; Denardin et al. 2006; Knobel et al. 2007),

$$T_B(H) = \frac{VK}{25k_B}\left[1 - \left(\frac{HM_S}{2K}\right)\right]^{3/2}, \quad (1)$$

where M_S is the saturation magnetization and K is the magnetic anisotropy (Ridier et al. 2017a). However, the random

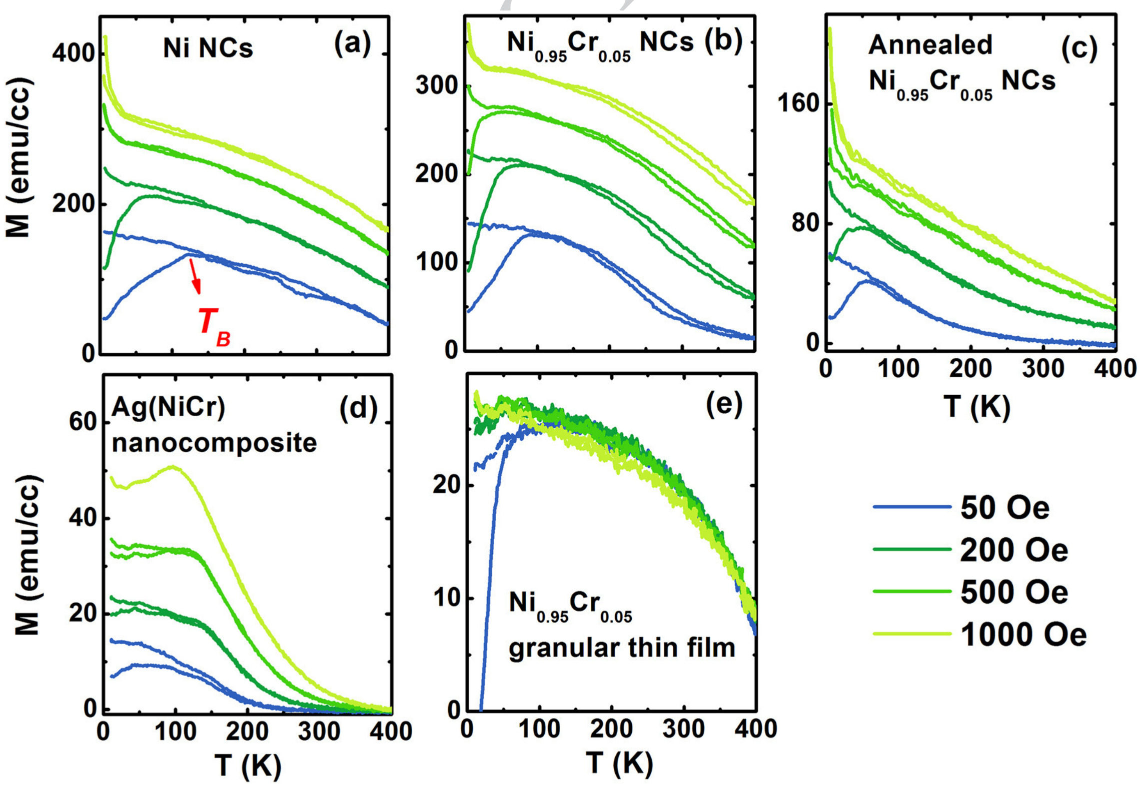

Fig. 2 M−T curves for **a** Ni NCs **b** $Ni_{0.95}Cr_{0.05}$ NCs **c** $Ni_{0.95}Cr_{0.05}$ annealed NCs **d** Ag(NiCr) nanocomposite and **e** $Ni_{0.95}Cr_{0.05}$ nanogranular films

anisotropy model (RAM) considers the interaction effects on the field dependence of $T_B(H)$. This model averages the anisotropy to an effective value (K_{eff}) within the correlation length (L_H) that defines the correlated volume (V_{eff}) over the number of correlated particles$N = \left[1 + x\frac{(L_H^3 - D^3)}{D^3}\right]$, where x is the volume fraction of the magnetic particles and D is their diameter (Fabris et al. 2019; Ridier et al. 2017a). RAM, thus, have two modifications, $K_{eff} = \frac{K}{\sqrt{N}}$, $V_{eff} = \frac{\pi}{6}ND^3$. The correlation length can be expressed as $L_H = D + \sqrt{\frac{2A_{eff}}{M_S H}}$, where A_{eff} is an exchange stiffness constant. Within this length scale, the exchange interactions can force the spin to align in polycrystalline materials. This L_H also depends on the applied magnetic field. When $L_H \rightarrow D$ (average particle diameter), then interactions become very weak, and these expressions tend to anisotropy and volume of an individual mono-dispersed particle, on the other hand, when$L_H \gg D$, it serves for the correlated particles. Now, on using K_{eff} andV_{eff}, expression (1) is reduced for coupled particles as.

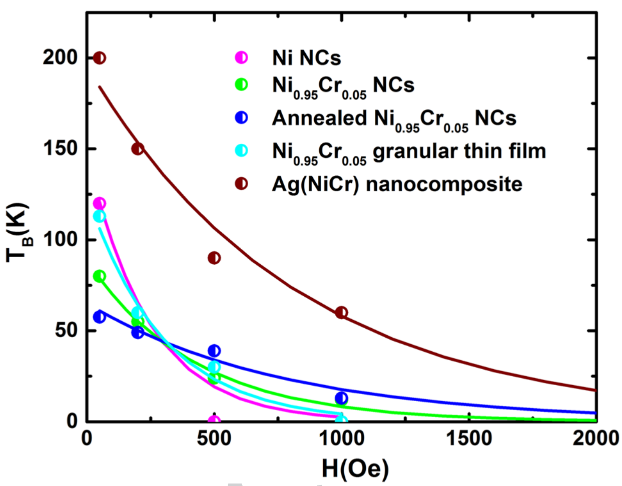

Fig. 3 Field dependence of the T_B(H) (experimental data represented by symbols) and fitted data with modified RAM (represented by solid lines)

$$T_B^{eff}(H) = \frac{K\pi D^3 N^{1/2}}{150k_B}\left[1 - \left(\frac{HM_S N^{1/2}}{2K}\right)\right]^{3/2} \quad (2)$$

We have plotted $T_{B\ vs.\ H}$ data in Fig. 3 for different types of NiCr nanostructures. The solid line in Fig. 3 is the best fit to the T_B vs H behavior. The corresponding fits were carried out considering $D = \sim 5$ nm, $x = \sim 35\%$ (estimated from TEM analysis in Fig. S1 – 9), $A = 1.6 \times 10^{-13}$ J/m (Ridier et al. 2017b) and M_S values (380–30 emu/cc) for different samples obtained from M–H loops at 30 K as a fixed parameter, while other free parameters (K and L_H) are summarized in Table. 1. The K values of Ni (9.57×10^4 J/m^3) and $Ni_{0.95}Cr_{0.05}$ (7.42×10^4 J/m^3) NCs are slightly different and have been attributed to the Cr segregations in the latter case, the stoichiometric $Ni_{0.95}Cr_{0.05}$ otherwise should show pronounced difference in values. The bulk Ni with [111] as the easy axis of magnetization has first-order cubic magnetocrystalline anisotropy constant $K_1 = -8 \times 10^4$ J/m^3 at low temperature (Goya et al. 2003; He et al. 2007). The magnetic anisotropy K is related to K_1 through the relation $K = K_1/12$ (Gittleman et al. 1974). Therefore, for pure Ni NCs, K_1 is extracted to be 11.4×10^5 J/m^3, which is one order larger than K_1 of bulk Ni. The possible source of increased magnetic anisotropy other than cubic magnetic anisotropy is surface anisotropy because shape anisotropy cannot be the main source of anisotropy considering the nearly spherical shape of present NCs (see TEM image). A likely situation is that there are ferromagnetic correlated regions in NCs whose magnetization directions are pinned or frozen by random anisotropy due to surface disorder. Interestingly, it is observed that the K value slightly decreases in annealed $Ni_{0.95}Cr_{0.05}$ NCs which can be due to predominant Cr segregation over particle aggregation that eventually weakens the magnetic coupling (Bohra et al. 2020). On the other hand, the high K value observed in AgNiCr nanocomposite is rather surprising because co-existing diamagnetic Ag matrix is anticipated to reduce the magnetic interaction among $Ni_{0.95}Cr_{0.05}$ grains. This unusual feature can be understood as follows: the interface between $Ni_{0.95}Cr_{0.05}$ grains and Ag metal matrix may undergo structural and orbital

Table 1 Fitting parameters (K and L_H) were obtained from the modified RAM. Other fitting parameters obtained by SPM + FM components for below T_B and SPM for above T_B

Sample	K(10^4 J/m^3)	L_H (nm) (at 200 Oe)	Below T_B(30 K)				Above T_B (200 K)
			M_{Sp} (emu/cc)	M_{Sf} (emu/cc)	B (%)	1—β (%)	M_{Sp} (emu/cc)
Ni NCs	9.57	11.48	344.10	421.10	29.41	70.59	359.60
$Ni_{0.95}Cr_{0.05}$ NCs	7.42	11.62	300.20	413.90	30.03	69.97	329.40
$Ni_{0.95}Cr_{0.05}$ annealed NCs	5.71	14.70	166.50	182.40	20.25	79.75	136.50
$Ni_{0.95}Cr_{0.05}$ nanogranular film	2.82	28.09	30.86	31.67	32.43	67.57	27.07
Ag(NiCr) nanocomposite	12.3	20.68	60.01	71.25	8.04	91.96	48.86

reconstructions which could result in the hybridization of 3d band orbitals of $Ni_{0.95}Cr_{0.05}$ surface atom with Ag, thus the enhancement of surface anisotropy, K_S (Bartolomé et al. 2008; Bohra et al. 2014) which in turn results in higher magnetic anisotropy; $K = K_{cubic} + 6\frac{K_S}{\langle D \rangle}$. In the absence of an Ag matrix, the system behaves like discontinuous nanogranular $Ni_{0.95}Cr_{0.05}$ films with lower K. The L_H calculated at 200 Oe is larger than the diameter D of the Ni and $Ni_{0.95}Cr_{0.05}$ NCs, indicating predominant dipole–dipole interactions. Further increase in L_H values for nanogranular $Ni_{0.95}Cr_{0.05}$ films and Ag(NiCr) nanocomposites are attributed to direct exchange interactions in the former and matrix-induced hybridization in the latter case. Our study shows that RAM analysis can also be used to extract the K values even for the strongly interacting regime, where the T_B of the individual nanostructures are hidden by the collective behavior.

After gaining knowledge about different types of interparticle magnetic interactions present among NiCr nanostructures, we examine how these interactions affect the shape of M–H loops. In Fig. 4, we have plotted the M–H loops for the various NiCr nanostructures at a temperature above and below T_B. Above T_B, we have not observed coercivity within the accuracy limit, while below T_B they show coercivity and remanence fields. The high coercivity H_C in Ag(NiCr) nanocomposites at low temperatures could be due to the increase in magnetic anisotropy K, discussed earlier. (See Table 1). However, the presence of coercivity in the order of a few Oersted above T_B can be due to the dipolar interaction effects. An analytical expression consisting of both ferromagnetic (FM) and superparamagnetic (SPM) components has been employed to identify the magnetic interactions (Ghosh et al. 2020; Saha et al. 2009; Singh et al. 2010) is given

$$M(H) = (1-\beta)\left\{\frac{2M_{Sf}}{\pi}\tan^{-1}\left[\frac{H \pm H_C}{H_C}\tan\frac{\pi S}{2}\right]\right\} + \beta\left\{M_{Sp}\left[\coth\left(\frac{\mu H}{k_B T}\right) - \frac{k_B T}{\mu H}\right]\right\} \quad (3)$$

Here, S is squareness ratio, M_{Sf} and M_{Sp} are FM and SPM saturation magnetization, respectively. Below T_B, M–H loops were well fitted with a combination of FM (first term) and SPM (second term) components, as shown (Fig. 4(a)). The H_C values obtained from the M–H loops were put as a fixed fit parameter that depends on the sample varying from

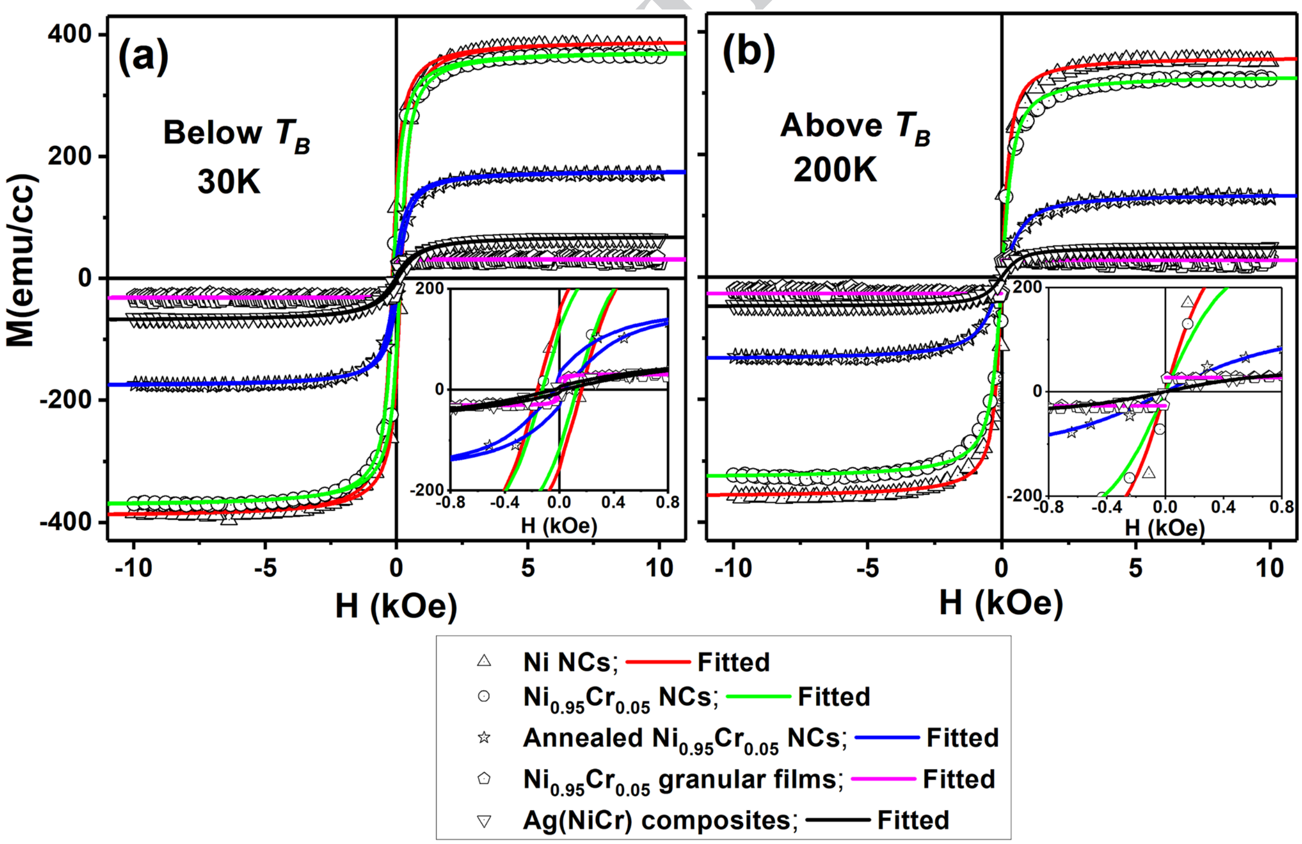

Fig. 4 M–H loops of various NiCr nanostructures **a** below T_B at 30 K and **b** above T_B at 200 K (plotted in symbols). Insets show M–H data near the origin. Former M–H loops were well fitted with SPM + FM contributions and later only with SPM (plotted in solid color lines)

Journal : Large 13204	Article No : 1998	Pages : 7	MS Code : 1998	Dispatch : 7-8-2021

18 to 170 Oe. The terms β and 1 – β refer to the SPM and FM contribution, respectively. The parameter β varies from 0 to 1. Parameters obtained from fittings are summarized in Table 1. The β value is found to vary from 8 to 32%, but ideally, in the blocking state, only FM contribution should occur. The lower β value in Ag(NiCr) nanocomposites infers that the Ag matrix prevents aggregation of $Ni_{0.95}Cr_{0.05}$ grains into bigger sizes, which means mostly smaller $Ni_{0.95}Cr_{0.05}$ grains are in SPM state for above T_B and in FM state below T_B. However, the presence of a slightly wide distribution of Ni and $Ni_{0.95}Cr_{0.05}$ NCs sizes can lead to two contributions namely 1) SPM and 2) FM phase, as bigger NCs remain frozen at successive low temperatures (Bohra et al. 2020). The highest M_{Sf} value of 421 emu/cc of Ni NCs is even less than the reported bulk Ni value of 485 emu/cc which may be linked with the random orientations of surface spins. These M_{Sf} values are in good agreement with M_S values obtained from the RAM model. Above T_B, the M–H loops (Fig. 4(b)) were fitted well to the SPM component with M_{Sp} value of 27–360 emu/cc. Thus, these observations strongly infer that the varying nature of interparticle interactions from dipole–dipole interaction to direct exchange or matrix-induced RKKY can have a different form of influence on hysteresis quantities M_R/M_{Sf}, H_C, and M_{Sf}.

Conclusion

This study aims at analyzing the competition of single-particle magnetic anisotropy and the interparticle interactions in NiCr nanostructures, i.e., NiCr dense nanoclusters, nanogranular NiCr thin films, and nanocomposites made of NiCr NCs in an Ag matrix. The blocking temperatures (T_B) extracted from FC and ZFC magnetization curves and their magnetic field dependence is analyzed using a random anisotropy model (RAM). Such a model considers the effect of magnetic interparticle interactions on the mere superparamagnetic behavior. The estimated magnetic anisotropy K ($2.82-12.3\times10^4$ J/m^3) values show the dependence on orbital hybridization, surface segregation, and interface character. This phenomenological model can successfully explain the different magnetic behavior in accordance with the magnetic components (FM, SPM, and PM) model for various NiCr nanostructures. This analysis may open a pathway towards understanding the underlying physics related to magnetic interactions in various technologically important gossamer M–Cr (M: Fe, Co, Ni) nano-systems.

Supplementary Information The online version contains supplementary material available at https://doi.org/10.1007/s13204-021-01998-y.

Acknowledgements The authors would like to thank Dr. R. E. Diaz (OIST, Japan) for her help with TEM measurements, and Dr. P. Grammatikopoulos (OIST, Japan) for useful discussion.

Declarations

Conflict of interests On behalf of all contributing authors, the corresponding author declares that they have no known competing financial interests or personal relationships that could have appeared to influence the work reported in this paper.

References

Andersson MS, Mathieu R, Lee SS, Normile PS, Singh G, Nordblad P, De Toro JA (2015) Size-dependent surface effects in maghemite nanoparticles and its impact on interparticle interactions in dense assemblies. Nanotechnol 26(47):475703. https://doi.org/10.1088/0957-4484/26/47/475703

Bartolomé J, García LM, Bartolomé F, Luis F, López-Ruiz R, Petroff F, Deranlot C, Wilhelm F, Rogalev A, Bencok P, Brookes NB (2008) Magnetic polarization of noble metals by Co nanoparticles in M-capped granular multilayers (M= Cu, Ag, and Au): An x-ray magnetic circular dichroism study. Phys Rev B 77(18):184420. https://doi.org/10.1103/PhysRevB.77.184420

Bitoh T, Makino A, Inoue A, Masumoto T (2003) Random anisotropy model for nanocrystalline soft magnetic alloys with grain-size distribution. Mater Trans 44(10):2011–2019. https://doi.org/10.2320/matertrans.44.2011

Bohra M, Singh V, Sowwan M, Bobo JF, Chung CJ, Clemens B (2014) Influence of packaging on the surface oxidation and magnetic properties of cobalt nanocrystals. J Phys d: Appl Phys 47(30):305002. https://doi.org/10.1088/0022-3727/47/30/305002

Bohra M, Grammatikopoulos P, Diaz RE, Singh V, Zhao J, Bobo JF, Kuronen A, Djurabekova F, Nordlund K, Sowwan M (2015) Surface segregation in chromium-doped NiCr alloy nanoparticles and its effect on their magnetic behavior. Chem Mater 27(9):3216–3225. https://doi.org/10.1021/acs.chemmater.5b00837

Bohra M, Singh V, Grammatikopoulos P, Toulkeridou E, Diaz RE, Bobo JF, Sowwan M (2016) Control of surface segregation in bimetallic NiCr nanoalloys immersed in Ag matrix. Sci Rep 6(1):1–8. https://doi.org/10.1038/srep19153

Bohra M, Grammatikopoulos P, Singh V, Zhao J, Toulkeridou E, Steinhauer S, Kioseoglou J, Bobo JF, Nordlund K, Djurabekova F, Sowwan M (2017) Tuning the onset of ferromagnetism in heterogeneous bimetallic nanoparticles by gas phase doping. Phys Rev Mater 1(6):066001. https://doi.org/10.1103/PhysRevMaterials.1.066001

Bohra M, Alman V, Showry A, Singh V, Diaz RE, Sowwan M, Grammatikopoulos P (2020) Aggregation vs surface segregation: antagonism over the magnetic behavior of NiCr nanoparticles. ACS Omega 5(51):32883. https://doi.org/10.1021/acsomega.0c03056

Denardin JC, Nunes WC, Knobel M (2006) Effects of magnetic interparticle coupling in the blocking temperature of granular Co multilayers. Phys b: Condens Matter 384(1–2):290–293. https://doi.org/10.1016/j.physb.2006.06.013

Dhayal V, Hashmi SZ, Kumar U, Choudhary BL, Kuznetsov AE, Dalela S, Kumar S, Kaya S, Dolia SN, Alvi PA (2020) Spectroscopic studies, molecular structure optimization and investigation of structural and electrical properties of novel and biodegradable Chitosan-GO polymer nanocomposites. J Mater Sci 55:14829–14847. https://doi.org/10.1007/s10853-020-05093-5

Fabris F, Tu KH, Ross CA, Nunes WC (2019) Influence of dipolar interactions on the magnetic properties of superparamagnetic particle systems. J Appl Phys 126(17):173905. https://doi.org/10.1063/1.5125595

Ghosh A, Srinivas V, Sundara R (2020) Comprehensive structural and magnetic properties of iron oxide nanoparticles synthesized through chemical routes. J Alloys Comp 818:152931. https://doi.org/10.1016/j.jallcom.2019.152931

Gittleman JI, Abeles B, Bozowski S (1974) Superparamagnetism and relaxation effects in granular Ni-SiO_2 and Ni-Al_2O_3 films. Phys Rev B 9:3891. https://doi.org/10.1103/PhysRevB.9.3891

Goya GF, Fonseca FC, Jardim RF, Muccillo R, Carreno NL, Longo E, Leite ER (2003) Magnetic dynamics of single-domain Ni nanoparticles. J Appl Phys 93(10):6531–6533. https://doi.org/10.1063/1.1540032

He L, Zheng W, Zhou W, Du H, Chen C, Guo L (2007) Size-dependent magnetic properties of nickel nanochains. Condens Matter, Phys. https://doi.org/10.1088/0953-8984/19/3/036216

Kaushik A, Dalela B, Rathore R, Vats VS, Choudhary BL, Alvi PA, Kumar S, Dalela S (2013) Influence of Co doping on the structural, optical and magnetic properties of ZnO nanocrystals. J Alloy Compd 578:328–335. https://doi.org/10.1016/j.jallcom.2013.06.015

Knobel M, Nunes WC, Winnischofer H, Rocha TC, Socolovsky LM, Mayorga CL, Zanchet D (2007) Effects of magnetic interparticle coupling on the blocking temperature of ferromagnetic nanoparticle arrays. J Non-Cryst Solids 353(8–10):743–747. https://doi.org/10.1016/j.jnoncrysol.2006.12.037

Knobel M, Nunes WC, Socolovsky LM, De Biasi E, Vargas JM, Denardin JC (2008) Superparamagnetism and other magnetic features in granular materials: a review on ideal and real systems. J Nanosci Nanotechnol 8(6):2836–2857. https://doi.org/10.1166/jnn.2008.15348

Kumar U, Upadhyay S, Alvi PA (2021) Study of reaction mechanism, structural, optical and oxygen vacancy-controlled luminescence properties of Eu-modified Sr_2SnO_4 Ruddlesden popper oxide. Physica B 604:412708. https://doi.org/10.1016/j.physb.2020.412708

Kumari A, Kumari K, Ahmed F, Alshoaibi A, Alvi PA, Dalela S, Ahmad MM, Aljawfi RN, Dua P, Vij A, Kumar S (2021) Influence of Sm doping on structural, ferroelectric, electrical, optical and magnetic properties of $BaTiO_3$. Vacuum 184:109872. https://doi.org/10.1016/j.vacuum.2020.109872

Mørup S, Hansen MF, Frandsen C (2010) Magnetic interactions between nanoparticles. Beilstein J Nanotechnol 1(1):182–190. https://doi.org/10.3762/bjnano.1.22

Muscas G, Concas G, Laureti S, Testa AM, Mathieu R, De Toro JA, Cannas C, Musinu A, Novak MA, Sangregorio C, Lee SS (2018) The interplay between single particle anisotropy and interparticle interactions in ensembles of magnetic nanoparticles. Phys Chem Chem Phys 20(45):28634–28643. https://doi.org/10.1039/C8CP03934H

Nunes WC, Socolovsky LM, Denardin JC, Cebollada F, Brandl AL, Knobel M (2005) Role of magnetic interparticle coupling on the field dependence of the superparamagnetic relaxation time. Phys Rev B 72(21):212413. https://doi.org/10.1103/PhysRevB.72.212413

Pacakova B, Mantlikova A, Niznansky D, Kubickova S, Vejpravova J (2016) Understanding particle size and distance driven competition of interparticle interactions and effective single-particle anisotropy. J Phys: Condens Matter 28(20):206004. https://doi.org/10.1088/0953-8984/28/20/206004

Petracic O, Chen X, Bedanta S, Kleemann W, Sahoo S, Cardoso S, Freitas PP (2006) Collective states of interacting ferromagnetic nanoparticles. J Magn Magn Mater 300(1):192–197. https://doi.org/10.1016/j.jmmm.2005.10.061

Punia K, Lal G, Barbar SK, Dolia SN, Alvi PA, Dalela S, Kumar S (2021a) Oxygen vacancies mediated cooperative magnetism in ZnO nanocrystals: A d0 ferromagnetic case study. Vacuum 184:109921. https://doi.org/10.1016/j.vacuum.2020.109921

Punia K, Lal G, Dalela S, Dolia SN, Alvi PA, Barbar SK, Modi KB, Kumar S (2021b) A comprehensive study on the impact of Gd substitution on structural, optical and magnetic properties of ZnO nanocrystals. J Alloy Compd 868:159142. https://doi.org/10.1016/j.jallcom.2021.159142

Ridier K, Gillon B, Chaboussant G, Catala L, Mazérat S, Rivière E, Mallah T (2017a) Individual-collective crossover driven by particle size in dense assemblies of superparamagnetic nanoparticles. Eur Phys J B 90(4):1–9. https://doi.org/10.1140/epjb/e2017-70534-9

Ridier K, Gillon B, Chaboussant G, Catala L, Mazérat S, Rivière E, Mallah T (2017b) Individual-collective crossover driven by particle size in dense assemblies of superparamagnetic nanoparticles. Eur Phys J B 90:77. https://doi.org/10.1140/epjb/e2017-70534-9

Saha R, Srinivas V, Rao TC (2009) Evolution of ferromagnetic like order in $Fe_2V_{1-x}Cr_xAl$ Heusler alloys. Phys Rev B 79(17):174423. https://doi.org/10.1103/PhysRevB.79.174423

Singh V, Srinivas V, Ranot M, Angappane S, Park JG (2010) Effect of polymer coating on the magnetic properties of oxygen-stabilized nickel nanoparticles. Phys Rev B 82(5):054417. https://doi.org/10.1103/PhysRevB.82.054417

Journal : Large 13204	Article No : 1998	Pages : 7	MS Code : 1998	Dispatch : 7-8-2021